

An improved high order finite difference method for non-conforming grid interfaces for the wave equation

Siyang Wang*

Abstract

This paper is an extension of a recently developed high order finite difference method for the wave equation on a grid with non-conforming interfaces. The stability proof of the previous method relies on the interface operators being *norm-contracting*, which is satisfied by the second and fourth order operators, but not by the sixth order operator. In this paper, we present a new way of numerical interface couplings to remove the *norm-contracting* requirement, so that the sixth order accurate scheme is also provably stable. Numerical experiments demonstrate the improved stability and accuracy property.

Keywords: Second order wave equation, Finite difference method, SBP-SAT, Non-conforming grid interfaces, Coupling, Multi-block

Mathematics Subject Classification: 65M06, 65M12

1 Introduction

Wave propagations can be modeled by hyperbolic partial differential equations (PDEs). When solving a hyperbolic PDE by a finite difference method, to achieve a certain accuracy a minimum number of grid points per wavelength is required. This number is smaller with a high order method than with a low order method, which makes high order finite difference methods more efficient to solve wave propagation problems on smooth domains [9, 12].

*Division of Scientific Computing, Department of Information Technology, Uppsala University, SE-751 05 Uppsala, Sweden. Email: siyang.wang@it.uu.se

On a uniform grid, high order central finite difference stencils are easily constructed by Taylor expansions [6]. Close to boundaries, one-sided stencils can be used. It is important that the boundary closure is accurate, and the numerical scheme is stable. One successful approach is to use a finite difference operator satisfying a summation-by-parts (SBP) property. When an SBP operator acts on a grid function, it mimics integration-by-parts principle in the continuous setting. An energy estimate can be obtained if boundary conditions are imposed appropriately, for example by using the simultaneous-approximation-term (SAT) method [3] or ghost points [23]. A scheme satisfying an energy estimate is called energy stable [7, 8].

When the computational domain has a complex geometry, to resolve the boundary feature the domain can be partitioned into blocks. Each block has four sides and is mapped to a reference domain. If the corners of adjacent blocks meet, we say they are conforming blocks; otherwise they are non-conforming. Similarly, a grid interface is conforming if no hanging nodes are present. When partitioning a domain, we can always make the blocks and interfaces conforming. However, in many situations it is desirable to use a more flexible strategy of partition that leads to non-conforming blocks and grid interfaces.

As an example, we consider a wave traveling in a heterogeneous medium with its wave speed varying in space. The wave length is proportional to the wave speed for a given frequency. For accuracy the grid spacing is determined by the shortest wavelength [9, 12]. If a uniform grid is used in the entire computational domain, then the grid spacing must be small enough to resolve the shortest wavelength, resulting in an unnecessarily fine grid elsewhere. It is then more efficient to construct a grid according to the wave length in each block, which leads to non-conforming interfaces with hanging nodes.

If only conforming blocks are allowed, the domain partitioning may end up with many blocks of small size. To use a high order finite difference method, a minimum number of grid points is required in each block due to the stencil width. This then results in unnecessarily many grid points in the small blocks, and consequently a suboptimal performance of the numerical scheme. In such a situation, non-conforming blocks are more appropriate.

Previous work on the numerical treatment of grid interfaces for the wave equation includes [26], where wave propagations in a heterogeneous medium with complex geometry are considered. A stable and accurate multi-block finite difference method with conforming grid interfaces and blocks is presented. The focus in [27] is the numerical treatment of non-conforming interfaces and blocks by using SBP-preserving interface operators: the interpolation operators [16] and projection operators [11]. Energy stability is proved with an assumption that the interface operators are *norm-contracting*.

In the same paper [27], it is verified that not all interface operators satisfy this assumption, and instability occurs when the sixth order method is used on a domain with non-conforming, curved interfaces.

In this paper, we construct new penalty terms in the SBP-SAT finite difference framework for the numerical interface treatment. The resulting scheme is energy stable even the interface operators are not *norm-contracting*. This extends the provably stable scheme from fourth order accuracy [27] to sixth order accuracy. Another contribution of this paper is the numerical treatment of non-conforming blocks and interfaces on curvilinear grids, where as in [27] such a case is studied on Cartesian grids. We also conduct numerical experiments to verify that the new sixth order scheme is stable with non-conforming, curved interfaces.

The paper is organized as follows. In Sec. 2, we introduce the SBP-SAT finite difference method. In Sec. 3 we consider the wave equation on a Cartesian grid and present the new penalty terms for numerical interface treatments. Stability is proved by the energy method. We then generalize the scheme to non-conforming blocks and grid interfaces on curvilinear grids in Sec. 4. Numerical experiments are performed in Sec. 5 to verify the accuracy property of the developed scheme. We draw conclusion in Sec. 6.

2 SBP-SAT finite difference method

Finite difference operators satisfying an SBP property have been widely used to discretize time dependent PDEs. An SBP operator has central finite difference stencils in the interior, and special one-sided stencils at a few grid points near boundaries. The boundary stencils are chosen so that the operator satisfies a summation-by-parts property, which is the discrete counterpart of integration-by-parts. With the SAT method imposing boundary and interface conditions, the SBP-SAT finite difference method possesses a great advantage: it is possible to prove energy stability for high order accurate schemes for initial-boundary-value problems.

To introduce the SBP-SAT finite difference method, we consider the one dimensional domain $[0, 1]$ discretized by the grid points $x_j = jh, j = 0, 1, \dots, N$ with a constant grid spacing $h = 1/N$. We use the capital letter, for example, U to denote a smooth function in $[0, 1]$, and the corresponding small letter, u , to denote its projection on the grid $u = [U(x_0), U(x_1), \dots, U(x_N)]^T$.

2.1 Definitions of SBP operators

The first derivative SBP operator $D_1 \approx \partial/\partial x$ is introduced in [14], and later refined in [24]. Formally it is defined as follows.

Definition 1. A difference operator $D_1 = H^{-1}Q$ approximating $\partial/\partial x$ is a diagonal norm first derivative SBP operator if H is diagonal positive definite and $Q + Q^T = \text{diag}(-1, 0, \dots, 0, 1)$.

The operator H defines the SBP norm, and leads to the identity

$$u^T H D_1 v = (D_1 u)^T H v - u_0 v_0 + u_N v_N,$$

which is the discrete analogue of integration-by-parts

$$\int_0^1 U V_x dx = - \int_0^1 U_x V dx - U(0)V(0) + U(1)V(1),$$

since the norm H is also a quadrature [4].

For the second derivative, we distinguish between a constant coefficient operator $D_2 \approx \partial^2/\partial x^2$ and a variable coefficient operator $D_2^{(b)} \approx \partial/\partial x(b(x)\partial/\partial x)$ with $b(x) > 0$.

Definition 2. A difference operator $D_2 = H^{-1}(-M + BS)$ approximating $\partial^2/\partial x^2$ is a diagonal norm second derivative SBP operator if H is diagonal positive definite, M is symmetric positive semi-definite, $B = \text{diag}(-1, 0, \dots, 0, 1)$, and the first and last row of S approximate $\partial/\partial x$ at boundaries.

Such an operator is constructed in [19]. It is later found in [2, 17] that the operator M in D_2 satisfies the following property.

Lemma 1. *The symmetric positive semi-definite operator M can be written as*

$$M = \tilde{M} + h\alpha(BS)^T BS$$

where \tilde{M} is also symmetric positive semi-definite, $\alpha > 0$ is a constant independent of h , B and S are the same as in Definition 2.

Lemma 1 is often referred to as the *borrowing trick*, and is essential for energy stability.

For the variable coefficient case we have correspondingly

Definition 3. A difference operator $D_2^{(b)} = H^{-1}(-M^{(b)} + B^{(b)}S)$ approximating $\partial/\partial x(b(x)\partial/\partial x)$ is a diagonal norm second derivative variable coefficients SBP operator if H is diagonal positive definite, $M^{(b)}$ is symmetric positive semi-definite, $B^{(b)} = \text{diag}(-b(x_0), 0, \dots, 0, b(x_N))$, and the first and last row of S approximate $\partial/\partial x$ at boundaries.

Such an operator is constructed in [16], and the operator $M^{(b)}$ satisfies a similar *borrowing trick* [26].

Lemma 2. *The symmetric positive semi-definite operator $M^{(b)}$ can be written as*

$$M^{(b)} = \tilde{M}^{(b)} + h\beta b_m (BS)^T BS$$

where \tilde{M} is also symmetric positive semi-definite, $\beta > 0$ is a constant independent of h , B and S are the same as in Definition 2, and

$$b_m = \min(b(x_0), b(x_1), \dots, b(x_l), b(x_N), b(x_{N-1}), \dots, b(x_{N-l}))$$

with a constant l independent of h .

We note that the constants α and β in Lemma 1 and 2 are independent of grid spacing, but depend on the order of accuracy of the SBP operator. The precise values of α and β can be found in [17, 27] and [26], respectively.

The definitions and precise forms of the above operators can be found in [14, 15, 16, 19, 24]. These operators have the minimal interior stencil width. In addition, they have the same associated norm H for a given accuracy order.

The interior stencil of an SBP operator is the standard central finite difference stencil with truncation error $\mathcal{O}(h^{2p})$. On a few grid points near boundaries, special one-sided stencils are used to fulfil the SBP requirement. With a diagonal norm H , the truncation error at the boundary points can at best be $\mathcal{O}(h^p)$ [14]. Operators D_1 and D_2 with $p = 1, 2, 3, 4$ are constructed in [14, 24] and [19], respectively. The variable coefficient operators $D_2^{(b)}$ with $p = 1, 2, 3$ are constructed in [15].

In this paper, we call the above SBP operators $2p^{\text{th}}$ order accurate. When using in a numerical scheme, we also call the scheme $2p^{\text{th}}$ order accurate, even though the truncation error of the numerical scheme may not be $\mathcal{O}(h^{2p})$ or $\mathcal{O}(h^p)$.

2.2 The SAT method

An SBP operator only approximates a certain derivative, but does not impose any boundary condition. The imposition of boundary conditions must lead to an energy estimate ensuring stability, which can be done by for example the SAT method [3], the projection method [20, 21, 22] and the ghost points method [23]. In this paper, we choose the SAT method to impose both boundary and interface conditions since in many cases it is easy to derive an energy estimate. The key ingredient of the SAT method is to add

penalty terms to the semi-discretized equation and choose penalty parameters properly so that an energy estimate is obtained. Detailed discussions of the SBP–SAT finite difference methods can be found in the two review papers [5, 25].

3 The wave equation on a Cartesian grid

We start by considering the wave equation in two space dimensions in a composite domain $\Omega = [0, 1]^2$ with an interface Γ at $x = 0.5$. The left and right domain are denoted by Ω_L and Ω_R , respectively. The equations governing the acoustic pressures are

$$U_{tt} = U_{xx} + U_{yy}, \quad (x, y) \in \Omega_L, \quad (1)$$

$$V_{tt} = V_{xx} + V_{yy}, \quad (x, y) \in \Omega_R. \quad (2)$$

At the interface the physical conditions are continuity of solutions and continuity of fluxes

$$U(0.5, y, t) = V(0.5, y, t), \quad U_x(0.5, y, t) = V_x(0.5, y, t). \quad (3)$$

For a wellposed problem, suitable boundary conditions must be imposed at the boundaries. As the focus in this paper is the numerical treatment of interface coupling, we exclude the discussions on boundary conditions and their numerical impositions. We refer to [13] for physical boundary conditions, and [18] for the numerical techniques.

To solve (1)–(3), we start by generating a Cartesian grid in each domain independently with $n_{xL} \times n_{yL}$ grid points in Ω_L and $n_{xR} \times n_{yR}$ grid points in Ω_R . We are particularly interested in the case $n_{yL} \neq n_{yR}$. Interface operators I_{L2R} and I_{R2L} are used for the grid coupling, where $L2R$ refers to *left to right* and $R2L$ refers to *right to left*. In the SBP–SAT finite difference framework, these operators are constructed in [11, 16], and they satisfy a *norm-compatible* condition.

Definition 4. Let H_{yL} and H_{yR} denote the SBP norms in the y -direction in Ω_L and Ω_R , respectively. The interface operators I_{L2R} and I_{R2L} are *norm-compatible* if

$$H_{yL}I_{R2L} = (H_{yR}I_{L2R})^T. \quad (4)$$

In [27], it is also defined that the interface operators are *norm-contracting* if the two matrices

$$H_{yL}(I_{yL} - I_{R2L}I_{L2R}) \quad \text{and} \quad H_{yR}(I_{yR} - I_{L2R}I_{R2L})$$

are symmetric positive semi-definite.

A stable SBP–SAT finite difference method for solving (1)–(3) is presented in [27]. Energy stability is proved by assuming the interface operators are *norm-compatible* and *norm-contracting*. While the *norm-compatible* condition is easily satisfied, the *norm-contracting* condition is not. Below we present a new way of imposing the interface conditions (3) with the advantage that an energy estimate is obtained without requiring the interface operators to be *norm-contracting*.

In this paper, we discretize (1)–(3) as

$$u_{tt} = \mathbf{D}_u u + SAT_{u1} + SAT_{u2} + SAT_{u3} + SAT_{\partial u}, \quad (5)$$

$$v_{tt} = \mathbf{D}_v v + SAT_{v1} + SAT_{v2} + SAT_{v3} + SAT_{\partial v}, \quad (6)$$

where

$$SAT_{u1} = \frac{1}{2} \mathbf{H}_{ux}^{-1} \mathbf{S}_{ux}^T (\mathbf{E}_{ux} u - (E_{LR} \otimes I_{R2L})v) \quad (7a)$$

$$SAT_{u2} = -\frac{\tau}{2} \mathbf{H}_{ux}^{-1} (\mathbf{E}_{ux} u - (E_{LR} \otimes I_{R2L})v) \quad (7b)$$

$$SAT_{u3} = -\frac{\tau}{2} \mathbf{H}_{ux}^{-1} ((E_{ux} \otimes (I_{R2L} I_{L2R}))u - (E_{LR} \otimes I_{R2L})v) \quad (7c)$$

$$SAT_{\partial u} = -\frac{1}{2} \mathbf{H}_{ux}^{-1} (\mathbf{E}_{ux} \mathbf{S}_{ux} u - (E_{LR} \otimes I_{R2L}) \mathbf{S}_{vx} v) \quad (7d)$$

and

$$SAT_{v1} = -\frac{1}{2} \mathbf{H}_{vx}^{-1} \mathbf{S}_{vx}^T (\mathbf{E}_{vx} v - (E_{RL} \otimes I_{L2R})u) \quad (8a)$$

$$SAT_{v2} = -\frac{\tau}{2} \mathbf{H}_{vx}^{-1} (\mathbf{E}_{vx} v - (E_{RL} \otimes I_{L2R})u) \quad (8b)$$

$$SAT_{v3} = -\frac{\tau}{2} \mathbf{H}_{vx}^{-1} ((E_{vx} \otimes (I_{L2R} I_{R2L}))v - (E_{RL} \otimes I_{L2R})u) \quad (8c)$$

$$SAT_{\partial v} = \frac{1}{2} \mathbf{H}_{vx}^{-1} (\mathbf{E}_{vx} \mathbf{S}_{vx} v - (E_{RL} \otimes I_{L2R}) \mathbf{S}_{ux} u) \quad (8d)$$

The numerical solution vectors u and v approximate the true solutions U and V , respectively. The Kronecker product \otimes is used to extend an operator in one space dimension to two space dimensions, and operators in two space dimensions are denoted by bold letters. The subscript of an operator indicates the spatial direction and the grid function that the operator is associated to. For example \mathbf{H}_{ux}^{-1} equals to $H_{ux}^{-1} \otimes I_{uy}$, where H_{ux}^{-1} is the inverse of the SBP norm in the x -direction acting on u , and I_{uy} is an identity operator. The operator \mathbf{E} extracts the numerical solution at the interface.

We compare the above scheme with the ones described in [26, 27] by discussing the penalty term SAT_u in (7a)–(7d). A term like $\mathbf{E}_{ux} u$ used in

[26, 27] is broken into two parts: $1/2\mathbf{E}_{ux}u$ in (7b) and $1/2E_{ux} \otimes I_{R2L}I_{L2R}u$ in (7c). Note the relation between them: $E_{ux} \otimes I_{R2L}I_{L2R}u$ is just $\mathbf{E}_{ux}u$ interpolated to the grid on the interface of Ω_R , then interpolated back to the grid of Ω_L . Since the interpolation is not exact, $E_{ux} \otimes I_{R2L}I_{L2R}u$ differs from $\mathbf{E}_{ux}u$ by the truncation error of the interface operators.

As stated in the following theorem, this change in penalty terms makes the method stable without requiring the interface operators to be *norm-contracting*.

Theorem 1. *The semi-discretization (5)–(6) is stable for any τ such that*

$$\tau \geq \max\left(\frac{1}{2\alpha h_{xL}}, \frac{1}{2\alpha h_{xR}}\right), \quad (9)$$

with a constant α in Lemma 1 if the interface operators are *norm-compatible*.

Proof. We prove stability by the energy method, that is, multiplying from the left of (5) by $u_t^T(H_{xL} \otimes H_{yL})$ and (6) by $v_t^T(H_{xR} \otimes H_{yR})$. By using the property of the SBP operator in Lemma 1, and the *norm-compatible* property (4) of the interface operator, we obtain the change of energy \mathbf{G}

$$\frac{d}{dt}\mathbf{G} = \frac{d}{dt}(\mathbf{G}_1 + \mathbf{G}_2 + \mathbf{G}_3) = 0, \quad (10)$$

where

$$\begin{aligned} \mathbf{G}_1 &= u_t^T(H_{xL} \otimes H_{yL})u_t + v_t^T(H_{xR} \otimes H_{yR})v_t \\ &\quad + u^T(H_{xL} \otimes M_{yL})u + v^T(H_{xR} \otimes M_{yR})v \\ &\quad + u^T(\tilde{M}_{xL} \otimes H_{yL})u + v^T(\tilde{M}_{xR} \otimes H_{yR})v, \\ \mathbf{G}_2 &= h_{xL}\alpha(\mathbf{E}_{0L}\mathbf{S}_{xL}u)\mathbf{H}_{yL}(\mathbf{E}_{0L}\mathbf{S}_{xL}u) \\ &\quad - (\mathbf{E}_{0L}\mathbf{S}_{xL}u)^T\mathbf{H}_{yL}(\mathbf{E}_{0L}u - (E_{LR} \otimes I_{F2C})v) \\ &\quad + \frac{\tau}{2}(\mathbf{E}_{0L}u - (E_{LR} \otimes I_{F2C})v)^T\mathbf{H}_{yL}(\mathbf{E}_{0L}u - (E_{LR} \otimes I_{F2C})v), \\ \mathbf{G}_3 &= h_{xR}\alpha(\mathbf{E}_{0R}\mathbf{S}_{xR}v)\mathbf{H}_{yR}(\mathbf{E}_{0R}\mathbf{S}_{xR}v) \\ &\quad - (\mathbf{E}_{0R}\mathbf{S}_{xR}v)^T\mathbf{H}_{yR}((E_{RL} \otimes I_{L2R})u - \mathbf{E}_{0R}v) \\ &\quad + \frac{\tau}{2}((E_{RL} \otimes I_{L2R})u - \mathbf{E}_{0R}v)^T\mathbf{H}_{yR}((E_{RL} \otimes I_{L2R})u - \mathbf{E}_{0R}v). \end{aligned}$$

Clearly, $\mathbf{G}_1 \geq 0$. By Young's inequality, we have $\mathbf{G}_2 \geq 0$ and $\mathbf{G}_3 \geq 0$ if $\tau \geq 1/(2\alpha h_{xL})$ and $\tau \geq 1/(2\alpha h_{xR})$, respectively. Therefore, the energy is conserved and the scheme is stable when (9) is satisfied. \square

We note that in the scheme developed in [27] the energy is greater or equal to \mathbf{G} in (10), with the inequality resulted from the *norm-contracting* condition.

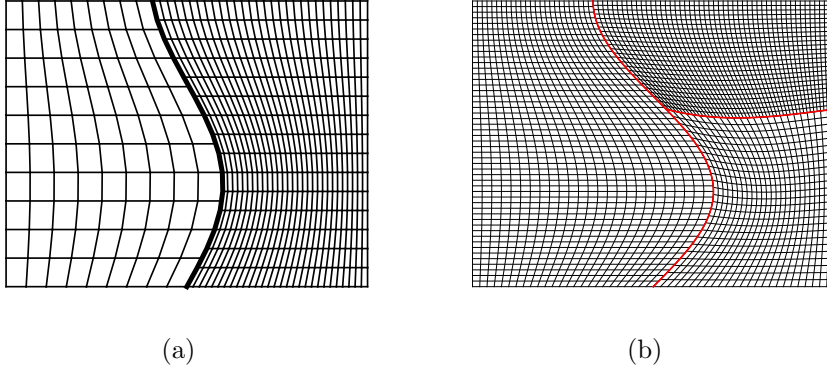


Figure 1: Non-conforming interfaces with (a) conforming blocks (b) non-conforming blocks

4 The wave equation on curvilinear grids

In this section, we generalize the scheme to curvilinear grids. We consider two cases: conforming blocks and non-conforming blocks illustrated in Figure 1a and 1b, respectively.

4.1 Numerical interface treatment of conforming blocks

With only conforming blocks in the domain, the corners of adjacent blocks meet. We consider again the domain $\Omega = [0, 1]^2$ but partitioned into two blocks Ω_L and Ω_R by a curved interface. The grids are then constructed independently in each block, see an illustration in Figure 1a. The grids in each block are mapped to a Cartesian grid in a logical domain. The governing equations are also transformed from the physical domain to the logical domain, and the computation is performed in the logical domain [10].

With the unknown variables U and V in Ω_L and Ω_R , the governing equations in the logical domain are

$$\begin{aligned} J_U U_{tt} &= (aU_x)_x + (cU_y)_y + (bU_y)_x + (bU_x)_y, \\ J_V V_{tt} &= (\alpha V_x)_x + (\gamma V_y)_y + (\beta V_y)_x + (\beta V_x)_y, \end{aligned} \quad (11)$$

where the Jacobians $J_U, J_V > 0$ and the variable coefficients satisfy $ac - b^2 > 0$ and $\alpha\gamma - \beta^2 > 0$. The interface conditions become

$$\begin{aligned} U &= V, \\ aU_x + bU_y &= \alpha V_x + \beta V_y, \end{aligned} \quad (12)$$

on $(x, y) \in \Gamma$. The coefficients in (11) depend on the geometry of the physical domain and the transformation, and the derivations are nicely presented in [1].

The equations (11) are then discretized by using the SBP operators, and the two blocks are patched together by the SAT method. The semi-discretized equations are

$$\begin{aligned} J_u u_{tt} &= \overline{(D_{2ux}^{(a)})} u + \overline{(D_{2uy}^{(c)})} u + \mathbf{D}_{1ux} \Lambda_b \mathbf{D}_{1uy} u + \mathbf{D}_{1uy} \Lambda_b \mathbf{D}_{1ux} u + SAT_u, \\ J_v v_{tt} &= \overline{(D_{2vx}^{(\alpha)})} v + \overline{(D_{2vy}^{(\gamma)})} v + \mathbf{D}_{1vx} \Lambda_\beta \mathbf{D}_{1vy} v + \mathbf{D}_{1vy} \Lambda_\beta \mathbf{D}_{1vx} v + SAT_v, \end{aligned} \quad (13)$$

where

$$\begin{aligned} SAT_u &= \frac{1}{2} \mathbf{H}_{ux}^{-1} \mathbf{H}_{uy}^{-1} [\Lambda_a \mathbf{E}_{ux} \mathbf{S}_{ux} + \Lambda_b \mathbf{E}_{ux} \mathbf{D}_{1uy}]^T \mathbf{H}_{uy} (\mathbf{E}_{ux} u - E_{LR} \otimes I_{R2L} v) \\ &\quad - \frac{\tau}{2} \mathbf{H}_{ux}^{-1} (E_{ux} \otimes I_{R2L} I_{L2R} u - E_{LR} \otimes I_{R2L} v) \\ &\quad - \frac{\tau}{2} \mathbf{H}_{ux}^{-1} (\mathbf{E}_{ux} u - E_{LR} \otimes I_{R2L} v) \\ &\quad - \frac{1}{2} \mathbf{H}_{ux}^{-1} ([\Lambda_a \mathbf{E}_{ux} \mathbf{S}_{ux} + \Lambda_b \mathbf{E}_{ux} \mathbf{D}_{1uy}] u - E_{LR} \otimes I_{R2L} [\Lambda_\alpha \mathbf{E}_{vx} \mathbf{S}_{vx} + \Lambda_\beta \mathbf{E}_{vx} \mathbf{D}_{1vy}] v). \end{aligned} \quad (14)$$

and

$$\begin{aligned} SAT_v &= -\frac{1}{2} \mathbf{H}_{vx}^{-1} \mathbf{H}_{vy}^{-1} [\Lambda_\alpha \mathbf{E}_{vx} \mathbf{S}_{vx} + \Lambda_\beta \mathbf{E}_{vx} \mathbf{D}_{1vy}]^T \mathbf{H}_{vy} (\mathbf{E}_{vx} v - E_{RL} \otimes I_{L2R} u) \\ &\quad - \frac{\tau}{2} \mathbf{H}_{vx}^{-1} (E_{vx} \otimes I_{L2R} I_{R2L} v - E_{RL} \otimes I_{L2R} u) \\ &\quad - \frac{\tau}{2} \mathbf{H}_{vx}^{-1} (\mathbf{E}_{vx} v - E_{RL} \otimes I_{L2R} u) \\ &\quad + \frac{1}{2} \mathbf{H}_{vx}^{-1} ([\Lambda_\alpha \mathbf{E}_{vx} \mathbf{S}_{vx} + \Lambda_\beta \mathbf{E}_{vx} \mathbf{D}_{1vy}] v - E_{RL} \otimes I_{L2R} [\Lambda_a \mathbf{E}_{ux} \mathbf{S}_{ux} + \Lambda_b \mathbf{E}_{ux} \mathbf{D}_{1uy}] u). \end{aligned} \quad (15)$$

We now clarify the notations in the semi-discretization (13).

1. The mixed-derivative terms: $(bU_y)_x$ is approximated by $\mathbf{D}_{1ux} \Lambda_b \mathbf{D}_{1uy} u$, where Λ_b is a diagonal matrix with diagonal entries the projection of $b(x, y)$ on the grid. The operators approximating the other three mixed-derivative terms are constructed in a similar way.
2. The variable-coefficient terms: In general the variable coefficients are functions of both x and y , therefore an operator approximating $(aU_x)_x$ cannot be constructed by a single Kronecker product, but as a sum

$$\overline{(D_{2ux}^{(a)})} = \sum_{i=1}^{n_{ux}} D_{2ux}^{a_i} \otimes E_{uy}^i,$$

where a_i is the projection of $a(x_i, y)$ on the grid, and E_{uy}^i has value one in entry (i, i) and zeros elsewhere. The second derivative operator $D_{2ux}^{a_i}$ is defined in Definition 2 with the associated M -operator satisfying Lemma 2. The operators approximating the other three variable coefficient terms are constructed in a similar way.

3. The penalty terms: The two interpolation operators I_{L2R} and I_{R2L} constructed in [11, 16] satisfy the *norm-compatible* condition

$$H_{uy}I_{R2L} = (H_{vy}I_{L2R})^T.$$

The energy stability of (13) follows in a very similar, but lengthy way as explained in [26] for the case with conforming interfaces. Instead of repeating the proof, we only show the main ideas.

We note that the energy stability proof of the semi-discretization (13) is identical to the one explained in [26] if the interface is conforming. For the more general case with non-conforming interfaces, with the penalty terms in (14)–(15) we eliminate the *norm-contracting* requirement of the interface operators in the same way as in Theorem 1. In addition, the penalty parameter τ needs to be large enough, as given in Theorem 1 in [26]. We note that the lower limit of τ for the curvilinear case is in a more complicated form than the lower limit for the Cartesian case (9). As for the curvilinear case, the lower limit of τ also depends on the geometry of the computational domain and the curvilinear mapping. We summarize the stability result in the following theorem.

Theorem 2. *There exists τ_0 such that for any $\tau \geq \tau_0$ the semi-discretization (13)–(15) is stable if the interface operators I_{L2R} and I_{R2L} are norm-compatible. τ_0 is inversely proportional to the mesh size, and is dependent on the domain geometry and curvilinear mapping.*

For accuracy, the SBP operators have truncation error $\mathcal{O}(h^{2p})$ in the interior and $\mathcal{O}(h^p)$ near the boundaries and interfaces. The interface operators constructed in [11, 16] have truncation error $\mathcal{O}(h^{2p})$ in the interior of an interface, and truncation error $\mathcal{O}(h^p)$ on a few grid points at the edge of an interface. Therefore, in the semi-discretization (13), the largest truncation error is $\mathcal{O}(h^{p-2})$ introduced by the first three penalty terms in (14) and (15) because of $\tau, \mathbf{H}_{ux}^{-1}, \mathbf{H}_{uy}^{-1} \sim \mathcal{O}(h^{-1})$. The truncation error $\mathcal{O}(h^{p-2})$ is only localized on a few number of grid points at the corner of two adjacent blocks. According to the accuracy analysis in [28], such a truncation error leads to an error $\mathcal{O}(h^{p+1})$ in the numerical solution. We can therefore expect a rate of convergence $p + 1$ of the semi-discretization (13), the same as the scheme developed in [27].

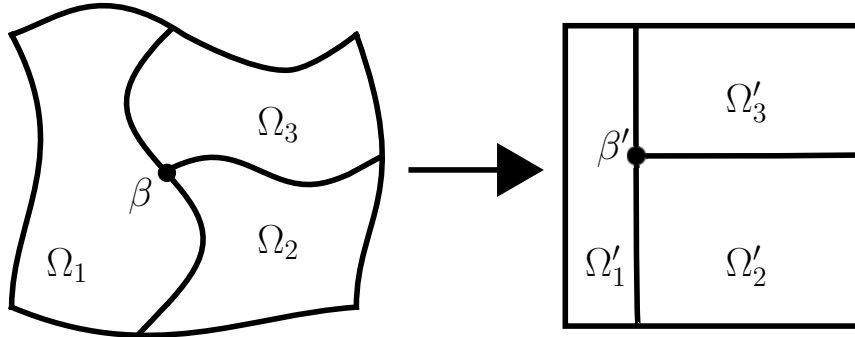


Figure 2: Transformation of a multi-block domain with a T-junction interface from the curvilinear coordinate to the Cartesian coordinate

4.2 Numerical interface treatment of non-conforming blocks

An example of non-conforming blocks is shown in Figure 1b. The lower left corner of the upper right domain sits in the middle of the right boundary of the left domain. Such an interface configuration is sometimes called a T-junction interface.

In the following we use Figure 2 for the discussion of mapping for non-conforming blocks. The three blocks Ω_1 , Ω_2 and Ω_3 meet at the point β . We further denote the interfaces $\Gamma_{12} = \Omega_1 \cap \Omega_2$, $\Gamma_{13} = \Omega_1 \cap \Omega_3$ and $\Gamma_{23} = \Omega_2 \cap \Omega_3$.

Coordinate transformation is performed block-wise, therefore an interface between two blocks is transformed twice. A common strategy is to transform each block in the physical domain to the unit square in the logical domain. This works well with conforming blocks. However, with nonconforming blocks such as in Figure 2 the interface Γ_{12} is transformed differently in Ω_1 and in Ω_2 , because Γ_{12} is an entire side of Ω_2 but only part of a side of Ω_1 . The same is true for the interface Γ_{13} , since the transformation in Ω_1 is different from that in Ω_3 . As a consequence, the transformed equation must be scaled [11]. In this paper, we use the following alternative coordinate transformation instead.

1. Choose Ω'_1 in a logical domain
2. Find the coordinates of β' in Ω'_1 , which corresponds to β in Ω_1 . Note that β' fixes the location of the left sides in Ω'_2 and Ω'_3 .

3. Transform Ω_1 , Ω_2 and Ω_3 to Ω'_1 , Ω'_2 and Ω'_3 , respectively.

With the above way of coordinate transformation, each interface is transformed in the same way in its adjacent two blocks. With the interface operators constructed as in (21)–(22) in [27], energy stability follows if the semi-discretization in each domain is formulated as in Sec. 4.1. This procedure can be easily generalized to more complicated multi-block structured grid.

5 Numerical experiments

In this section, numerical experiments are performed to verify the stability and accuracy property of the numerical schemes developed in this paper. We solve the wave equation on the domain depicted in Figure 1b. The composite domain is $[-1, 1] \times [0, 1]$ and the interface in the vertical direction is defined by $x = \sin(3\pi y/2)/3$. The intersection point (\bar{x}, \bar{y}) of the two interfaces is chosen by letting $\bar{y} = 0.621$. The interface in the horizontal direction is defined by $y = \sin(\pi x/2)/5 + \bar{y} - \sin(\pi \sin(3\pi \bar{y}/2)/6)/5$. The numbers of grid points in the left, lower right and upper right domain are 26×52 , 26×26 and 51×26 , respectively. Both the blocks and interfaces are non-conforming, see a close-up in Figure 3a. When refining the mesh, the number of grid points is doubled in each spatial direction in every domain.

To test accuracy and rate of convergence, we use the manufactured solution

$$U = \cos(3\pi x + 1) \cos(4\pi y + 2) \cos(5\pi t + 3). \quad (16)$$

to obtain initial and Neumann boundary data, and propagate the wave until $t = 2$. With this analytical solution, there is no forcing term in the equation.

We solve the equation by the fourth and sixth order SBP–SAT finite difference method, and use the classical Runge–Kutta method to integrate in time. The time step is chosen small enough so that the error in the solution is determined by the spatial discretization. The errors in L_2 norm are shown in Figure 3b, and the associated rates of convergence are given at the end of each error plot. In the figure, we use *new SAT* as the legend to denote the results obtained by the scheme in this paper, and *old SAT* to denote the result obtained by the scheme in [27]. The x -axis label N is the number of grid points in the x -direction in the left domain.

We observe that the fourth and sixth order accurate scheme lead to third and fourth order convergence rate, respectively. This agrees well with the accuracy discussion in the end of Sec. 4.1 in this paper. We note that the sixth order method gives much smaller error than the fourth order methods.

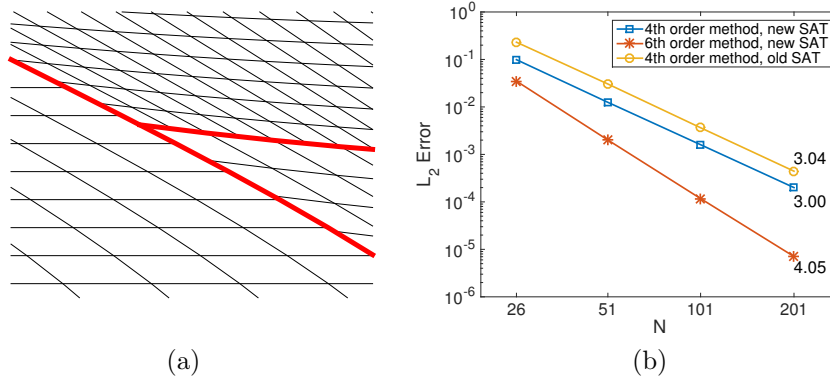


Figure 3: (a) A close-up of the interfaces (b) Rate of convergence

In addition, the four order method developed in this paper gives a smaller error than the fourth order method in [27]. We have also performed an experiment with the sixth order method in [27] and the numerical solution quickly blows up, indicating that method is unstable. This is not surprising because the energy analysis in [27] requires the *norm-compatible* condition of the interface operators, which are not satisfied by the sixth order operators.

6 Conclusion

We use the SBP-SAT finite difference method to solve the wave equation on a composite domain. The domain is divided by curved interfaces resulting in non-conforming blocks, and the grid is constructed in each block independently resulting in non-conforming grid interfaces. We develop new penalty terms to patch the blocks together by the SAT method. The sixth order accurate scheme in [27] is unstable on curvilinear grids. With the new penalty terms presented in this paper the scheme is provably stable. Numerical experiments demonstrate the superiority of the new sixth order accurate scheme. In addition, we find that the new fourth order accurate scheme is more accurate than the fourth order accurate scheme in [27].

Acknowledgement

The author thanks Professor Gunilla Kreiss for help in the work leading to this paper.

References

- [1] M. ALMQUIST, I. KARASALO AND K. MATTSSON, *Atmospheric sound propagation over large-scale irregular terrain*, J. Sci. Comput., 61(2014), pp. 369–397.
- [2] D. APPELÖ AND G. KREISS, *Application of a perfectly matched layer to the nonlinear wave equation*, Wave Motion, 44(2007), pp. 531–548.
- [3] M. H. CARPENTER, D. GOTTLIEB AND S. ABARBANEL, *Time-stable boundary conditions for finite-difference schemes solving hyperbolic systems: methodology and application to high-order compact schemes*, J. Comput. Phys., 111(1994), pp. 220–236.
- [4] D. C. DEL REY FERNÁNDEZ, P. D. BOOM AND D. W. ZINGG, *A generalized framework for nodal first derivative summation-by-parts operators*, J. Comput. Phys., 266(2014), pp. 214–239.
- [5] D. C. DEL REY FERNÁNDEZ, J. E. HICKEN AND D. W. ZINGG, *Review of summation-by-parts operators with simultaneous approximation terms for the numerical solution of partial differential equations*, Comput. & Fluids, 95(2014), pp. 171–196.
- [6] B. FORNBERG, *Calculation of weights in finite difference formulas*, SIAM Rev., 40(1998), pp. 685–691.
- [7] B. GUSTAFSSON, *High Order Difference Methods for Time Dependent PDE*, Springer-Verlag, Berlin Heidelberg, 2008.
- [8] B. GUSTAFSSON, H. O. KREISS AND J. OLIGER, *Time-Dependent Problems and Difference Methods*, Wiley, New Jersey, 2013.
- [9] T. HAGSTROM AND G. HAGSTROM, *Grid stabilization of high-order one-sided differencing II: second-order wave equations*, J. Comput. Phys., 231(2012), pp. 7907–7931.
- [10] P. KNUPP AND S. STEINBERG, *Fundamentals of Grid Generation*, CRC Press, 1993.
- [11] J. E. KOZDON AND L. C. WILCOX, *Stable coupling of nonconforming, high-order finite difference methods*, SIAM J. Sci. Comput., 38(2016), pp. A923–A952.
- [12] H. O. KREISS AND J. OLIGER, *Comparison of accurate methods for the integration of hyperbolic equations*, Tellus XXIV, 24(1972), pp. 199–215.

- [13] H. O. KREISS, O. E. ORTIZ AND N. A. PETERSSON, *Initial-boundary value problems for second order systems of partial differential equations*, ESAIM–Math. Model. Num., 46(2012), pp. 559–593.
- [14] H. O. KREISS AND G. SCHERER, *Finite element and finite difference methods for hyperbolic partial differential equations*, Mathematical aspects of finite elements in partial differential equations, Symposium proceedings (1974), pp. 195–212.
- [15] K. MATTSSON, *Summation by parts operators for finite difference approximations of second-derivatives with variable coefficient*, J. Sci. Comput., 51(2012), pp. 650–682.
- [16] K. MATTSSON AND M. H. CARPENTER, *Stable and accurate interpolation operators for high-order multiblock finite difference methods*, SIAM J. Sci. Comput., 32(2010), pp. 2298–2320.
- [17] K. MATTSSON, F. HAM AND G. IACCARINO, *Stable and accurate wave-propagation in discontinuous media*, J. Comput. Phys., 227(2008), pp. 8753–8767.
- [18] K. MATTSSON, F. HAM AND G. IACCARINO, *Stable boundary treatment for the wave equation on second-order form*, J. Sci. Comput., 41(2009), pp. 366–383.
- [19] K. MATTSSON AND J. NORDSTRÖM, *Summation by parts operators for finite difference approximations of second derivatives*, J. Comput. Phys., 199(2004), pp. 503–540.
- [20] K. MATTSSON AND J. NORDSTRÖM, *High order finite difference methods for wave propagation in discontinuous media*, J. Comput. Phys., 220(2006), pp. 249–269.
- [21] P. OLSSON, *Summation by parts, projections, and stability. I*, Math. Comput., 64(1995), pp. 1035–1065.
- [22] P. OLSSON, *Summation by parts, projections, and stability. II*, Math. Comput., 64(1995), pp. 1473–1493.
- [23] N. A. PETERSSON AND B. SJÖGREEN, *Stable grid refinement and singular source discretization for seismic wave simulations*, Commun. Comput. Phys., 8(2010), pp. 1074–1110.
- [24] B. STRAND, *Summation by parts for finite difference approximations for d/dx* , J. Comput. Phys., 110(1994), pp. 47–67.

- [25] M. SVÄRD AND J. NORDSTRÖM, *Review of summation-by-parts schemes for initial-boundary-value problems*, J. Comput. Phys., 268(2014), pp. 17–38.
- [26] K. VIRTA AND K. MATTSSON, *Acoustic wave propagation in complicated geometries and heterogeneous media*, J. Sci. Comput., 61(2014), pp. 90–118.
- [27] S. WANG, K. VIRTA AND G. KREISS, *High order finite difference methods for the wave equation with non-conforming grid interfaces*, J. Sci. Comput., 68(2016), pp 1002–1028.
- [28] S. WANG, A. NISSEN AND G. KREISS, *Convergence of finite difference methods for the wave equation in two space dimensions*, arXiv:1702.01383.